*Journal of Engineering Physics and Thermophysics, Vol. 80, No. 4, 2007*

## OPTICAL METHODS IN THERMOPHYSICAL MEASUREMENTS

# STATISTICAL ANALYSIS OF SPECKLE FIELDS IN DIGITAL LASER MONITORING OF THE MICROSTRUCTURE OF PAPER

**V. V. Azharonok,[a] N. B. Bazylev,[b] E. I. Lavinskaya,[b] I. I. Filatova,[a] and N. A. Fomin[b]**

UDC 535.311+536.24

*It has been shown that digital dynamic speckle photography is an effective method for quantitative diagnostics of changes in the structure of paper processed by pulsed discharge. A theory of the dynamic statistics of speckle fields and mathematical relations are given. In using optical magnification $\mathfrak{M} = 1$, the software developed permits fast statistical processing of up to 250,000 microzones in a two-dimensional CCD image of size 20 × 30 mm. The results obtained point to a high spatial and temporal resolution of the method and the possibility of its real-time realization. It has been shown that noise filtering is an important part of speckle image processing. The software permits filtering both in direct calculation of the correlation function and in the Fourier plane with the use of the fast Fourier transform.*

**Introduction.** Monitoring of the internal structure of materials is a traditional problem of diagnostics, in solving which a wide experience has been gained. For various problems on these lines, along with optical methods, acoustic, X-ray, induction, and other methods as well as their combinations are used successfully [1].

Before the advent of lasers optical diagnostic techniques found wide application and gained deserved recognition in many directions of scientific research due to their numerous advantages, the most important of which are the nonperturbative character of measurements, high spatial and temporal resolution, zero lag, high accuracy, and informativeness [2, 3]. This also holds for diagnostics based on the registration and analysis of the radiation scattered by the investigated medium [4–6]. Diagnostics with the use of scattered radiation becomes especially attractive when turning to the analysis of the microstructure of an *inhomogeneous semitransparent medium*. In the first works on scattering, such media, with account for single scattering, were called "turbid," and media in which the processes of multiple scattering are significant are called "highly turbid" ones (see, e.g., [4, 5]). Paper of thickness 20–200 μm is a typical example of a "highly turbid" medium and serves as a good generator of speckle fields. Later such media were called inhomogeneous, randomly inhomogeneous, dispersive, polydispersive, etc., since it is precisely optical inhomogeneities of the internal structure of a medium with a spatial scale of the order of the radiation wavelength that are the cause of light scattering. The nature of such optical inhomogeneities can be entirely different. Inhomogeneities of the complex refractive index can be due to both foreign bodies (water droplets and specks of dust in the atmosphere, suspensions and emulsions, foreign inclusions in transparent media) and fluctuations of the molecular density and orientation that change the dielectric constant of the medium [6, 7].

A powerful impetus to the development of optical diagnostic techniques was given by the discovery of laser systems and their wide reduction to practice of measurements (see, e.g., [8–11]). With the advent of lasers, work on optical diagnostics in diffuse coherent radiation in the presence of clearly defined speckle fields underwent development [12–16]. Initially, the appearance of speckles (microspots) on optical images was treated as undesirable noise. Many researchers tried to suppress this noise. However, in the early 1970s, mainly upon the publication of the results of the experiments conducted by Burch and Tokarskii [17], new potentialities of practical use of speckle distributions

[a]Institute of Molecular and Atomic Physics, National Academy of Sciences of Belarus, 70 Nezalezhnost' Ave., Minsk, 220072; [b]A. V. Luikov Heat and Mass Transfer Institute, National Academy of Sciences of Belarus, 15 P. Brovka Str., Minsk, 220072, Belarus. Translated from Inzhenerno- Fizicheskii Zhurnal, Vol. 80, No. 4, pp. 127–137, July–August, 2007. Original article submitted August 26, 2006.

1062-0125/07/8004-0769

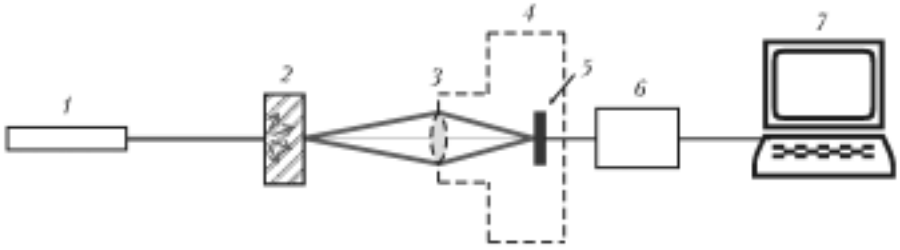


Fig. 1. Block-diagram of the experimental speckle tomograph of the structure of semitransparent inhomogeneous media: 1) probing laser; 2) investigated diffuse object (paper); 3) speckle field imaging optical system; 4) digital camera; 5) high-resolution CCD matrix; 6) optical memory; 7) personal computer.

of the laser intensity in novel measuring technologies opened up. Methods for investigating dispersive media based on the analysis of temporal fluctuations of scattered radiation, often called methods of *optical shift*, *correlation or dynamic spectroscopy*, as well as the laser-Doppler method, similar to the above-mentioned ones, in which fluctuations of the scattered radiation frequencies are analyzed, became popular [18–21]. The methods of dynamic speckle interferometry include analysis of both temporal and spatial fluctuations of the radiation scattered by a dispersive medium (see, e.g., [15]).

Below we propose a simple method for investigating the microstructure of a stationary scattering medium based on the statistical analysis of only spatial fluctuations (speckle fields) in the laser radiation scattered by the medium. The application of this approach is based on the digital technique of radiation recording with a high spatial resolution and direct recording in the PC memory of speckle fields, from whose statistical analysis quantitative information about the microstructure of the investigated medium is extracted. As our investigations have shown, the proposed method is a reliable tool for monitoring changes in the microstructure of paper upon its processing by the plasma of pulsed low-current discharge.

**Experimental Facility.** The structural changes in the investigated samples of paper were diagnosed by their probing with a narrow laser beam. A speckle field was generated directly in the sample being investigated as a result of the three-dimensional interference of the multiply scattered coherent radiation and projected by the imaging optical system on a high-resolution CCD matrix in much the same way as in diagnosing microflows in *micro-PIV* [22] and in diagnosing biotissues by the method of laser *dynamic speckle interferometry* [23] (see Fig. 1).

The laser radiation was focused directly on the sample, as is shown in Fig. 2a, or was supplied by means of an optical fiber (see Fig. 2b). Analysis of the data obtained was carried out by calculating the statistical functions of the first and second orders. Averaging was carried out over a small zone of the CCD matrix containing a sufficient number of working cells (pixels), and the image in each pixel of the camera is formed as a result of the total scattering in the control volume in the sample into the solid angle $\Omega$. Thus, in each zone (averaging window) the set of statistical functions characterizing the local microstructure of the investigated sample was determined. The speckle field obtained was recorded by a Nikon D70S CCD camera (Japan) containing 3008 × 2000 pixels on a 20 × 30-mm matrix.

*The spatial resolution* of measurements is determined by the sizes of the averaging windows, by which autocorrelation analysis of the recorder speckle field is performed. With optical magnification $\mathfrak{M} = 1$ and averaging over the minimal windows containing 5 × 5 or 7 × 7 pixels the limiting spatial resolution is about 50 μm in simultaneous monitoring of the whole object of size 20 × 30 mm. Importantly, as this field decreases with increasing number of $\mathfrak{M}$, the spatial resolution can be markedly increased. In measurements of an object of size 2 × 3 mm, the optical magnification can amount to $\mathfrak{M} = 10$ and the spatial resolution will be about 5 μm. In Prof. Meinhart's works [24, 25], optical magnification $\mathfrak{M} = 100$ realized with the aid of a Nikon ECLIPSE E 600FN microscope is used. Such an optical configuration permitted obtaining, even on a relatively small matrix of 1280 × 1024 pixels, an image of a speckle field with sizes of 415 × 415 μm and a spatial resolution of about 1 μm. An insignificant further improvement of the spatial resolution is possible if the averaging windows are closed, which makes it possible to increase 2–4 times the number of vectors being determined (see below). The above quantities pertain to the spatial resolution of microstruc-

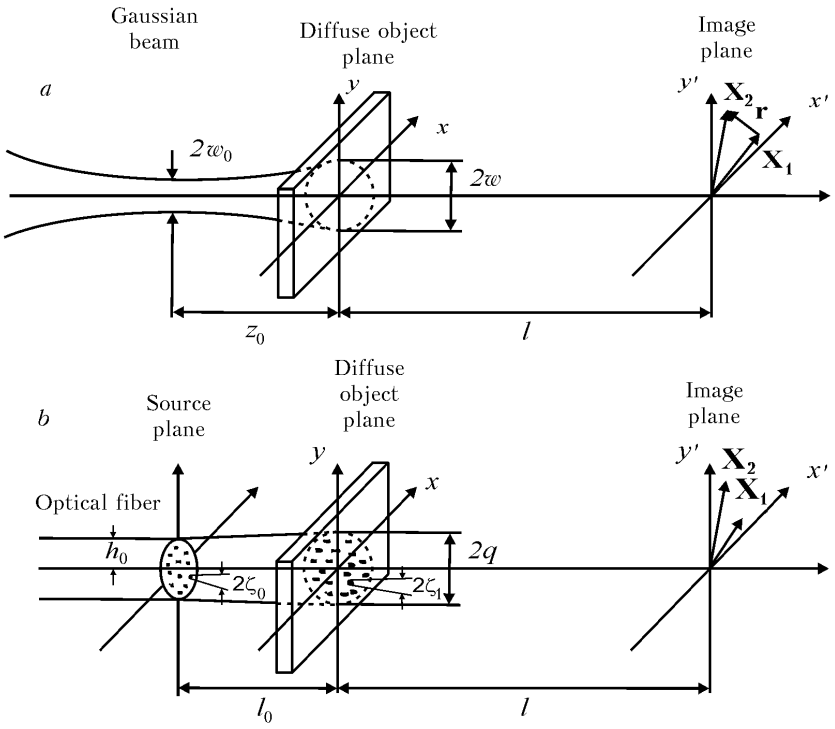


Fig. 2. Speckle field formation under radiation scattering by a diffuse object illuminated by a laser source with Gaussian intensity distribution (a) and a source with "limited" Gaussian distribution (b).

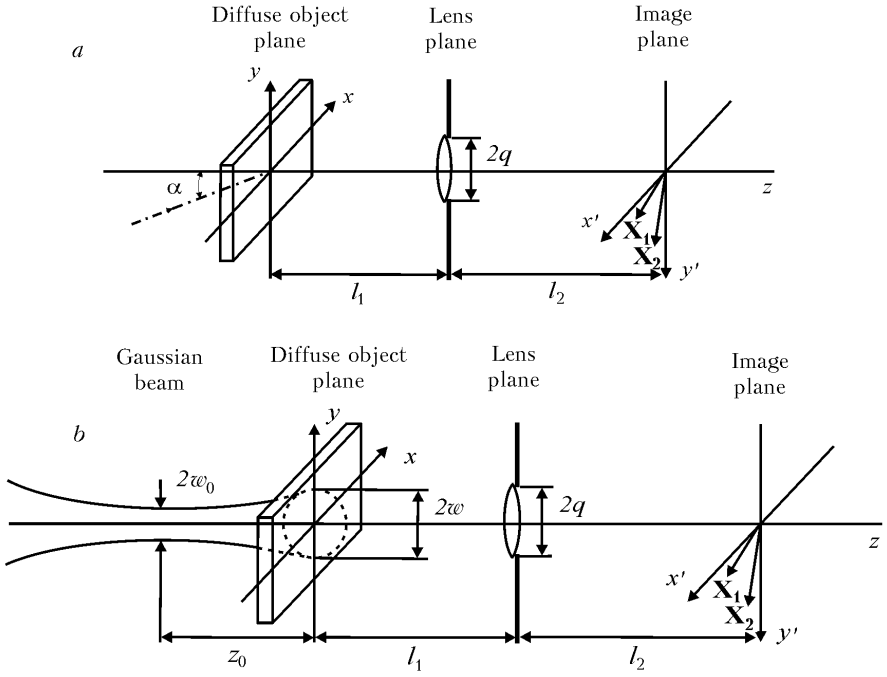


Fig. 3. Speckle field formation on the CCD matrix under radiation scattering by a diffuse object with the help of a single-lens optical system when the object is illuminated by a collimated laser source (a) and a laser source with Gaussian intensity distribution (b).

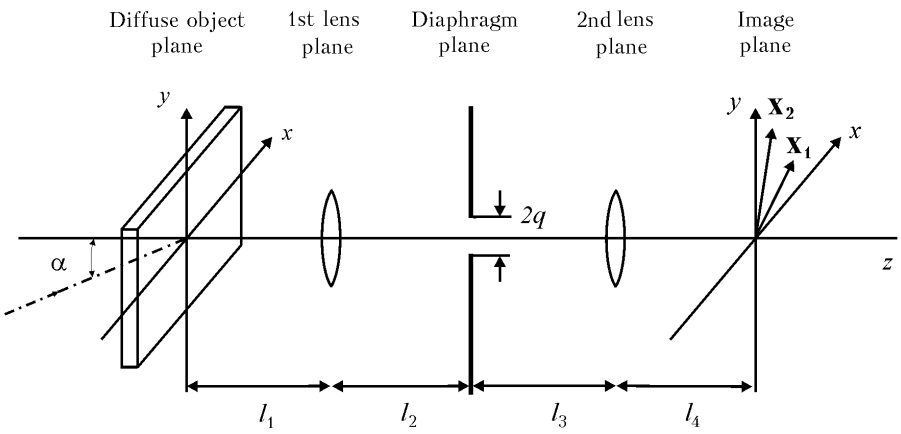


Fig. 4. Speckle field formation on the CCD matrix with the help of a two-lens optical system with the investigated diffuse object illuminated by a collimated laser source.

TABLE 1. Signal-to-Noise Ratio in the Image Focus under Volume Illumination of the Scattering Centers

| Depth of focus $\delta z$, μm | Concentration of scattering centers (by volume) $N_v$, % | | | |
|---|---|---|---|---|
| | 0.01 | 0.02 | 0.04 | 0.08 |
| 25 | 2.2 | 2.1 | 2.0 | 1.9 |
| 50 | 1.9 | 1.7 | 1.4 | 1.2 |
| 125 | 1.5 | 1.4 | 1.2 | 1.1 |
| 170 | 1.3 | 1.2 | 1.1 | 1.0 |

ture variations within the limits of the sample being investigated. The spatial scales of the registered changes in the microstructure of the investigated samples are much lower and lie in the submicron range. The optical magnification in macrophotography was adopted to the investigated object by means of the optical systems shown in Figs. 3 and 4.

*The depth of focus* in imaging through the optical system, a microscope, is determined by the relation (see [24, 26])

$$\delta z = \frac{\tilde{n}\lambda_0}{\mathrm{NA}^2} + \frac{\tilde{n}\delta_{\mathrm{px}}}{\mathfrak{M}\mathrm{NA}} = \delta z_{\mathrm{d}} + \delta z_{\mathrm{g}} . \tag{1}$$

Substituting NA = $\tilde{n}a/f$ and $\lambda_0 = \tilde{n}\lambda$ into (1), we obtain the estimate of the diffraction term in relation (1) $\delta z_{\mathrm{d}} \approx \lambda\tilde{n}(f/a)^2$. Accordingly, the geometrical correction will have the form $\delta z_{\mathrm{g}} \approx \delta_{\mathrm{px}} f/\mathfrak{M}a$. For the size of the registered inhomogeneity $d_{\mathrm{p}} \geq \delta_{\mathrm{px}}/\mathfrak{M}$, in [24] a simple engineering relation for the depth of focus

$$\delta z = \frac{3\lambda_0}{\tilde{n}a^2} f^2 + 2.16 d_{\mathrm{p}} \left( \frac{1}{\tan \Theta} \right) \tag{2}$$

was obtained. The results of the calculations of noises by these relations for media with a small volume fraction of scattering centers are given in Table 1. These data show that for the chosen image geometry averaging of the results of measurements on the $z$-axis occurs in most cases over the whole thickness of the investigated samples of paper.

*The temporal resolution* of monitoring is determined by the laser characteristics, the measuring circuit, and the technical parameters of the camera and the processor. In using a pulse-periodic laser, the temporal resolution is determined by the minimal time interval between successive lasing pulses, the frequency of image storage by the CCD camera, and the time of correlation analysis of obtained images on the PC. Optimization of the software makes it pos-

TABLE 2. Average Size of Speckles $r_s$ and Transfer Functions of the Optical System $r_0$ and $r_i$ for Different Optical Configurations (Figs. 2–4)

| Optical configuration | Formulas for calculating optical system parameters | | |
|---|---|---|---|
| Fig. 2a | $r_s = \frac{2l}{k_0 w}$ | — | — |
| Fig. 2b | $r_s = \frac{l}{l_0}\zeta_0$ | — | — |
| Fig. 3a | $r_s = \frac{2l_2}{k_0 q}$ | $r_0 = \frac{1}{2} r_s (1+\theta_1^2)^{1/2}$ | $r_i = \frac{l_1}{k_0 q}(1+\theta_1^2)^{1/2}$ |
| Fig. 3b | $r_s = \frac{2l_2}{k_0 q}$ | $r_0 = \frac{1}{2} r_s (1+\theta_1^2)^{1/2}$ | $r_i = \frac{l_1}{k_0 q}(1+\theta_1^2)^{1/2}$ |
| Fig. 4 | $r_s = \frac{2}{k_0 q}\left(l_3 + l_4 - \frac{l_3 l_4}{F_2}\right)$ | $r_0 = \frac{1}{2} r_s (1+\theta_2^2)^{1/2}$ | $r_i = \frac{l_1 l_2 A_1}{k_0 q}(1+\theta_2^2)^{1/2}$ |
| Fig. 4, $l_2 = F_2$, $l_3 = F_2$ | $r_s = \frac{2F_2}{k_0 q}$ | $r_0 = \frac{1}{2} r_s (1+\theta_3^2)^{1/2}$ | $r_i = \frac{F}{k_0 q}(1+\theta_3^2)^{1/2}$ |

sible to realize real- or quasi-real-time processing of images with a frequency of obtaining processed results equal to 1–25 Hz [27].

**Statistical Processing of Measurement Data.** A speckle field is formed in scattered light as a result of the interference of all beams hitting a given point. It is assumed that by virtue of the object diffusivity the phase differences of all these beams are uniformly distributed in the range from 0 to 2π. Let $\mathbf{x} = \mathbf{x}(x, y)$ be the Cartesian coordinates in the object plane and $\mathbf{X} = \mathbf{X}(x', y')$ be the coordinates in the image (viewing) plane (see Figs. 2–4). When a plane diffuse object is illuminated by a stationary light wave having a complex amplitude $\mathbf{E}_0 = \mathbf{E}_0(\mathbf{x})$, the complex amplitude of the scattered wave in the detection plane will be defined by the transfer function of the optical system $\mathbf{K} = \mathbf{K}(\mathbf{x}, \mathbf{X})$

$$\mathbf{E}(\mathbf{X}, t) = \int \mathbf{E}_0(\mathbf{x}, t) \times \mathbf{K}(\mathbf{x}, \mathbf{X})\, dx\,. \tag{3}$$

To analyze more complex optical configurations, let us introduce, for simplicity of recording, one-dimensional transfer functions of the optical system $r_i = |\mathbf{K}(0, \mathbf{X})|^2$ and $r_0 = |\mathbf{K}(0, \mathbf{X})|^2$ (Table 2). For a lens-free geometry (see Fig. 2), the full transfer function is given as

$$\mathbf{K}(\mathbf{x}, \mathbf{X}) = \frac{k}{i2\pi l} \exp\left(ik \frac{|\mathbf{x} - \mathbf{X}|^2}{2l}\right) \exp(ikl)\,. \tag{4}$$

For a one-lens optical configuration, this function is written as [28]

$$\mathbf{K}(\mathbf{x}, \mathbf{X}) = \frac{-k^2 q^2}{4\pi i l_1 l_2} \exp\left[\frac{-k^2 q^2}{4(1+\theta_1^2)}\left|\frac{\mathbf{x}}{l_1} - \frac{\mathbf{X}}{l_2}\right|^2\right] \exp\left\{i\left[k\left(l_1 + l_2 + \frac{|\mathbf{x}|^2}{2l_1} + \frac{|\mathbf{X}|^2}{2l_2}\right) + \right.\right.$$

$$\left.\left. + \tan^{-1}\theta_1 - \frac{k^2 q^2 \theta_1}{4(1+\theta_1^2)}\left|\frac{\mathbf{x}}{l_1} - \frac{\mathbf{X}}{l_2}\right|^2\right]\right\}. \tag{5}$$

The parameters $l_1$, $l_2$ and $q$ are given in Fig. 3, and $\theta_1 = \frac{kq^2}{2}\left(\frac{1}{l_1} + \frac{1}{l_2} - \frac{1}{F}\right)$.

For a more complex imaging system consisting of two lenses, as is shown in Fig. 4, the transfer function is of the form

$$\mathbf{K}(\mathbf{x}, \mathbf{X}) = \frac{-k^2 q^2}{4\pi i l_1 l_2 l_3 l_4 A_1 A_2 (1+\theta_2^2)^{1/2}} \exp\left[\frac{-k^2 q^2}{4(1+\theta_2^2)} \left|\frac{\mathbf{x}}{A_1 l_1 l_2} - \frac{\mathbf{X}}{A_2 l_3 l_4}\right|^2\right] \times$$

$$\times \exp\left\{i\left[k\left(l_1 + l_2 + l_3 + l_4 - i\tan^{-1}\theta_2\right) + i\frac{k}{2}\left[\frac{1}{l_1}\left(1 - \frac{1}{A_1 l_1}\right)|\mathbf{x}|^2 + \frac{1}{l_4}\left(1 - \frac{1}{A_2 l_4}\right)|\mathbf{X}|^2\right] - \right.\right. \tag{6}$$

$$\left.\left. - i\frac{k^2 q^2 \theta_2^2}{4(1+\theta_2^2)} \left|\frac{\mathbf{x}}{A_1 l_1 l_2} - \frac{\mathbf{X}}{A_2 l_3 l_4}\right|^2\right]\right\}.$$

Here $A_1 = \frac{1}{l_1} + \frac{1}{l_2} - \frac{1}{F_1}$; $A_2 = \frac{1}{l_3} + \frac{1}{l_4} - \frac{1}{F_2}$; $\theta_2 = \frac{kq^2}{2}\left(\frac{1}{l_2} + \frac{1}{A_1 l_2^2} - \frac{1}{A_2 l_3^2}\right)$.

The first-order statistical functions for a speckle field are expressed in terms of the probability density of the intensity distribution $p_I(I)$. For an ideal speckle field, this function obeys the Gaussian statistics:

$$p_I(I) = \begin{cases} \frac{1}{\sqrt{2\pi}\,\sigma_I} \exp\left(-\frac{I}{2\sigma_I^2}\right), & I \geq 0; \\ 0, & I < 0. \end{cases} \tag{7}$$

With the aid of this function the speckle field contrast

$$\mathbb{C} = \frac{\sigma_I}{\langle I \rangle} \tag{8}$$

can be defined.

In digital recording of the field with the aid of the CCD matrix, the laser radiation intensity can be given in the matrix form $I(p', q')$, and the contrast value can be determined by direct calculation in each window $(m, n)$ of averaging by the formula

$$\mathbb{C}(m, n) = \frac{\sigma_I(m, n)}{\langle I(m, n)\rangle} = \frac{\sqrt{\langle I(m, n)^2\rangle - \langle I(m, n)\rangle^2}}{\langle I(m, n)\rangle} =$$

$$= \frac{\sqrt{\frac{1}{MN}\sum_{p'=1}^{M}\sum_{q'=1}^{N}\left[I^{m,n}(p', q')\right]^2 - \left[\frac{1}{MN}\sum_{p'=1}^{M}\sum_{q'=1}^{N} I^{m,n}(p', q')\right]^2}}{\frac{1}{MN}\sum_{p'=1}^{M}\sum_{q'=1}^{N} I^{m,n}(p', q')}, \tag{9}$$

where $\sigma_I(m, n)$ is the rms deviation of the intensity in the window. In the ideal speckle field, this value is equal to the average speckle field intensity $\sigma_I(m, n) = \langle I(m, n)\rangle$, and the contrast $\mathbb{C}(m, n) = 1$. When the statistics is disturbed, e.g., due to a change in the microstructure of the object being investigated, the field contrast changes and the microstructure modification can be characterized quantitatively by the changes in the contrast.

The second-order statistical functions are the most general forms of describing the spatial-temporal variations of speckle fields [29]. For the fluctuating component $\Delta I = I - \langle I\rangle$ of the radiation intensity in the speckle field, the space-time autocorrelation function $\mathfrak{J}_{\Delta I}$ can be given as follows:

$$\Im_{\Delta I}(\mathbf{X}_1, \mathbf{X}_2, t_1, t_2) = \langle \Delta I(\mathbf{X}_1, t_1)\, \Delta I^*(\mathbf{X}_2, t_2) \rangle . \tag{10}$$

The autocorrelation function for the complex wave amplitude is defined as

$$\Im_E(\mathbf{X}_1, \mathbf{X}_2, t_1, t_2) = \langle E(\mathbf{X}_1, t_1)\, E^*(\mathbf{X}_2, t_2) \rangle . \tag{11}$$

These functions characterize the cross correlation of the two fields obtained at different points in the space and at different instants of time, and upon adequate normalization they vary in the range from 0 to 1.

An important second-order statistical function is also the so-called radiation *power spectrum* defined as a Fourier transform of the corresponding autocorrelation function (see [15]). According to the Wiener–Khinchin theorem, this function can be expressed as follows:

$$\mathfrak{A}_E(\nu, \omega) = \left(\frac{1}{2\pi}\right)^{1/2} \int \Im_E(r, \tau) \exp(-i\nu r) \exp(-i\omega\tau)\, dr d\tau , \tag{12}$$

where $\omega = |\omega| = [\omega_x^2 + \omega_y^2]^{1/2}$, but $\nu = |\nu| = [\nu_x^2 + \nu_y^2]^{1/2}$ and $r = |\mathbf{r}| = [(\Delta x)^2 + (\Delta y)^2]^{1/2}$.

Restricting ourselves to the consideration of only the spatial fluctuations, we will represent these functions for an ideal speckle field formed by a lens of diameter $D_\mathrm{L}$ as

$$\Im_{\Delta I}(r) = \langle I \rangle^2 \left[ 1 + \left| 2 \frac{J_1\left(\frac{\pi D_\mathrm{L} r}{\lambda z}\right)}{\frac{\pi D_\mathrm{L} r}{\lambda z}} \right|^2 \right],$$

$$\mathfrak{A}_I(\nu) = \langle I \rangle^2 \left\{ \delta(\nu_x, \nu_y) + \left(\frac{\lambda z}{D_\mathrm{L}}\right)^2 \frac{4}{\pi} \left[ \cos^{-1}\left(\frac{\lambda z}{D_\mathrm{L}} \nu\right) - \frac{\lambda z}{D_\mathrm{L}} \nu \sqrt{1 - \left(\frac{\lambda z}{D_\mathrm{L}} \nu\right)^2} \right] \right\}. \tag{13}$$

Let us denote by $r_\mathrm{h}$ the characteristic correlation size for the structure of the investigated object. For the generation of speckle fields with Gaussian statistics, it is necessary that in the volume $\pi r_\mathrm{h}^2 d_\mathrm{h}$ only one scattering center is situated and that such centers are uniformly distributed over the entire diffuse object. Then

$$\Im_E = \pi r_\mathrm{h}^2 \int E_0(\mathbf{x}_1, t_1)\, E_0^*(\mathbf{x}_1, t_2)\, K(\mathbf{x}_1, \mathbf{X}_1)\, K^*(\mathbf{x}_1, \mathbf{X}_2)\, d\mathbf{x}_1 . \tag{14}$$

The diffuse object can be illuminated by lasers with different intensity distributions over the object surface. The most common case is the Gaussian distribution

$$\mathbf{E}_0(\mathbf{x}, t) = \frac{w_0}{w} \left[ -\frac{|\mathbf{x}|^2}{w^2} - i\left( w_0 t - k_0 z - \frac{\pi}{\lambda \rho} |\mathbf{x}|^2 - \varphi_0 \right) \right]. \tag{15}$$

The quantities $w$ and $\rho$ here denote the radii of the laser beam and the wavefront curvature, and the quantities with subscripts 0 denote the parameters in the region of the waist (in "focus") as is shown in Fig. 2a. For a laser source with the Gaussian intensity distribution in the waist region the laser beam radius and the wavefront curvature will be defined by the following relations: $w = w_0 \left[ 1 + \left( \frac{z}{z'} \right)^2 \right]^{1/2}$ and $\rho = z \left[ 1 + \left( \frac{z'}{z} \right)^2 \right]$, where $z' = \frac{\pi}{\lambda} w_0^2$.

With allowance for the measurement error the autocorrelation function in the window being considered can be defined as

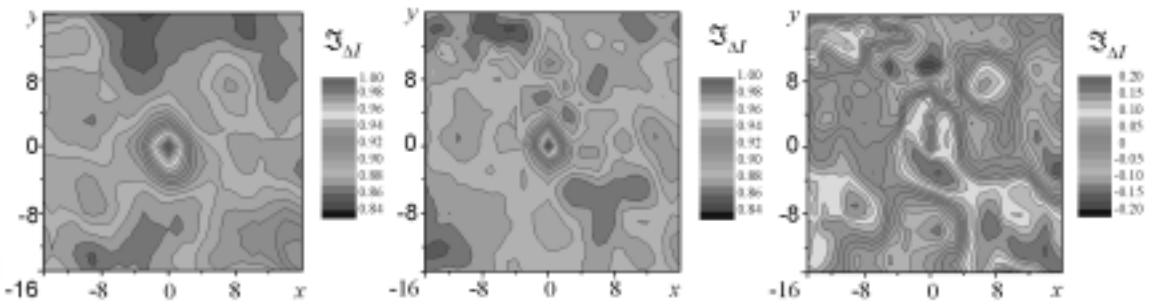

Fig. 5. Sections of the spatial autocorrelation function of the speckle field generated by the paper before processing (at the center) and after processing by pulsed discharge plasma (on the left). On the right, the difference isolines of the obtained functions are shown.

$$\Im_{\Delta I} = I \otimes I^{*} + \sigma_{\mathrm{n}} . \tag{16}$$

In the Fourier plane, this relation will have the form

$$\mathbb{F}\left\{\Im_{\Delta I}\right\} = \mathbb{F}\left\{I\right\}\mathbb{F}\left\{I^{*}\right\} + \tilde{\sigma}_{\mathrm{n}} , \tag{17}$$

and the estimate of the sought autocorrelation function $\tilde{\Im}_{\Delta I}$ is obtained by the relation

$$\tilde{\Im}_{\Delta I} = \mathbb{F}^{-1}\left\{\mathbb{F}\left\{\tilde{I}\right\}\mathbb{F}\left\{\tilde{I}^{*}\right\}\right\}. \tag{18}$$

The function $\Im_{\Delta I}(m, n)$ can be calculated by direct comparison of the corresponding intensities:

$$\Im_{\Delta I}(m, n) = \frac{MN}{(M-n)(N-n)}\left[\frac{\sum\limits_{p'=1}^{M-mN-n}\sum\limits_{q'=1} I(p', q')\, I(m+p', n+q')}{\sum\limits_{p'=1}^{M}\sum\limits_{q'=1}^{N}\left(I(p', q')\right)^{2}}\right]. \tag{19}$$

**Results and Discussion.** Figures 5–7 give various statistical functions of speckle fields and their modifications upon processing of the speckle field generators — paper samples — by a pulsed low-current discharge. The typical three-dimensional autocorrelation function of the speckle field being analyzed has a clearly defined maximum at the origin of coordinates and rapidly decreases upon receding from it. The circle diameter in the section of this function as it decreases by a factor of 2.71 (denoted below as $D_{\infty}$) characterizes the average size of speckles (in pixels) in the recording plane. Let us denote as $\langle d_{\infty}\rangle$ the average statistical size of speckles in the field generated by the unprocessed paper and as $\langle d\rangle = (\langle d_x\rangle^2 + \langle d_y\rangle^2)^{1/2}$ in the speckle field generated by the processed sample [22]. Upon optical processing of the specklograms the Fourier transform of the single-exposure specklogram represents a diffraction halo formed after the specklogram upon its scanning by a laser beam. The halo obtained is not modulated by the interference fringes as in the case of the double-exposure specklogram. Consequently, these sections represent either concentric circles for the isotropic samples or ellipses with the direction of the semimajor axis orthogonal to the direction of the dominant deformation of speckles in investigating the processed samples. In optical processing, the measured parameters in each specklogram window are semiaxes of the diffraction halo ellipse $D_x$, $D_y$. In the presence of anisotropy, the values of these semiaxes can be different. As mentioned above, these values or, to be more precise, their differences from the diameter of the initial speckle field diffraction halo $D_{\infty}$ are proportional to the deformation window-averaged difference of the elongation of speckles along the corresponding orthogonal axes $\langle \Delta d_x\rangle = \langle d_x - d_{\infty}\rangle$, $\langle \Delta d_y\rangle = \langle d_y - d_{\infty}\rangle$:

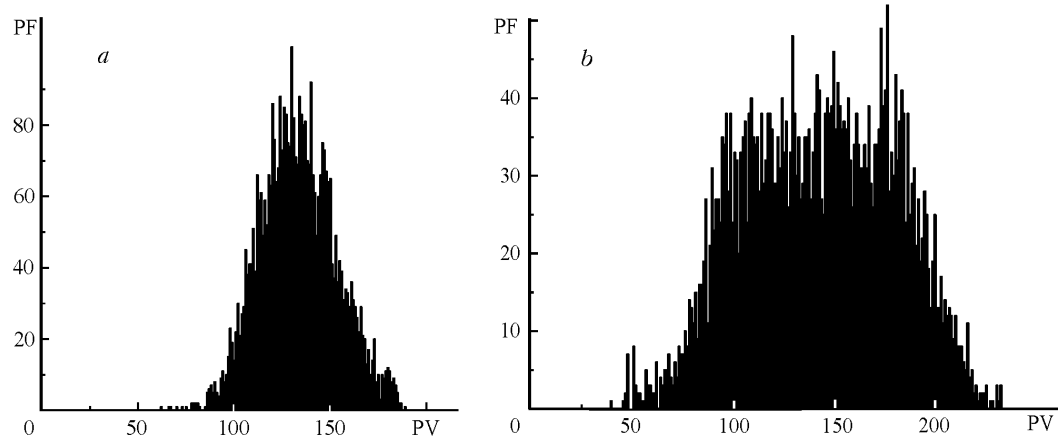


Fig. 6. Probability distribution density for the intensity in the speckle field upon processing of the speckle field generator — a paper sample — by pulsed discharge plasma for different processing regimes: a) by helium plasma; b) by nitrogen plasma.

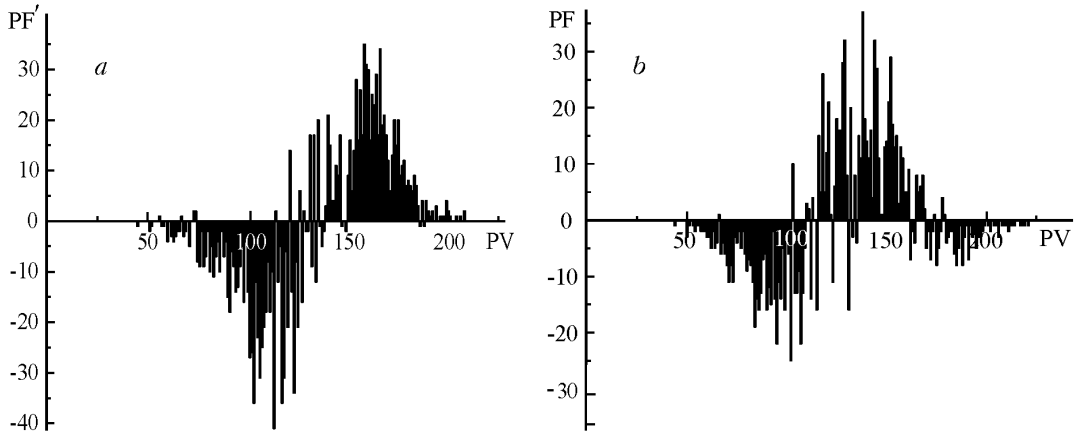


Fig. 7. Differences of the probability distribution density for the intensity in the speckle field of the control paper sample and after its processing by pulsed discharge plasma for different processing regimes: a) upon processing by helium plasma; b) upon processing by nitrogen plasma.

$$\frac{D_\infty(m,n)}{D_x(m,n)} = C_1 \frac{\langle d_x\rangle(m,n)}{\langle d_\infty\rangle(m,n)} = C_1 \frac{\langle \Delta d_x\rangle(m,n) + \langle d_\infty\rangle(m,n)}{\langle d_\infty\rangle(m,n)}, \tag{20}$$

$$\frac{D_\infty(m,n)}{D_y(m,n)} = C_1 \frac{\langle d_y\rangle(m,n)}{\langle d_\infty\rangle(m,n)} = C_1 \frac{\langle \Delta d_y\rangle(m,n) + \langle d_\infty\rangle(m,n)}{\langle d_\infty\rangle(m,n)}. \tag{21}$$

In digital processing of images, the values of $D_x$ and $D_y$ are determined directly by the calculated autocorrelation function.

Analysis of the data presented in Fig. 5 shows that in paper processing the spatial autocorrelation function undergoes marked changes, which points to a considerable modification of the microstructure of the investigated sample. The processing conditions were chosen so that no apparent changes in the structure are observed with the aid of the microscope. The difference between the correlation functions in the maximum reaches 20% of the correlation function in the peak, which is more than enough for reliable monitoring of the change in the microstructure of samples in their

processing by the low-current pulsed discharge plasma. Analysis of the spatial distribution of this difference (Fig. 5, on the right) shows that upon modification of the structure its anisotropy markedly increases.

Figure 6 shows the probability density distributions for the intensity in speckle fields under different conditions of paper processing. Analysis of the data presented shows that histograms are also a convenient form of presentation of the results of statistical processing of speckle fields for monitoring changes in the microstructure of analyzed samples. The difference between the histograms at individual points reaches 40% of the initial value and permits positive identification of processed parts of the paper.

**Conclusions.** The possibility of quantitative diagnostics of changes in the microstructure of scattering media with the use of statistical analysis of numerically registered speckle fields generated by the investigated samples has been shown. The software developed makes it possible to recover up to 250,000 vectors of the spatial deformation of speckle fields in a two-dimensional region of size 20 × 30 mm in imaging a speckle field with magnification $\mathfrak{M} = 1$. The size of the investigated region can be reduced by a factor of 10–100 with the use of microoptics with the necessary magnification. In the proposed configuration, the spatial resolution in the measurement plane is about 100 μm. On the coordinate along the optical beam, averaging of the information over the whole thickness of the sample (20–200 μm) occurs. The use of tomographic methods for reconstructing the microstructure [31] is the topic of future studies.

The authors thank O. G. Penyaz'kov for support and helpful discussions, and P. P. Khramtsov and S. P. Rubnikovich for useful recommendations and assistance in performing experiments and developing programs for mathematical processing of images, as well as the INTAS and the NAS of Belarus for financing part of the work with grants and projects INTAS 03-51-3332, "Vodorod-19," "Nanotech 1.13," and "Thermal processes-25."

## NOTATION

$a$, object radius, m; $A_1$, $A_2$, coefficients, $m^{-1}$; $C_1$, normalizing factor; $d$, size of speckles in the field generated by the processed sample, μm; $D_x$, $D_y$, semiaxes of the diffraction halo ellipse, m; $D_\infty$, diameter of the diffraction halo ellipse of the initial speckle field, m; $d_\infty$, size of speckles in the field generated by the unprocessed sample, μm; $d_h$, characteristic correlation depth, m; $d_p$, size of recorded inhomogeneity, μm; $\Delta d_x$, $\Delta d_y$, difference characteristics of the elongation of speckles along the corresponding axes, μm; $D_L$, lens diameter, m; $\mathbf{E}_0$, complex amplitude vector of the stationary wave, V; $\mathbf{E}(\mathbf{X}, t)$, complex amplitude vector of the wave, V; $E$, modulus of the complex amplitude of the wave, V; $f$, focal length of the objective, m; $F$, $F_1$, $F_2$, focal lengths of the lenses, m; $h_0$, fiber radius, μm (see Fig. 2b); $i$, imaginary unit; $I(m, n)$, laser radiation intensity in the speckle field, W/m$^2$; $I^*(m, n)$, transposed laser radiation intensity in the speckle field, W/m$^2$; $J_1(...)$, first-order Bessel function; $k_0$, $k$, wave numbers, $cm^{-1}$; $\mathbf{K}(\mathbf{x}, \mathbf{X})$, transfer function of the optical system; $l$, distance from the object plant to the image plane, m; $l_0$, distance from the source plane to the image plane, m; $M$, $N$, sizes of the discretization domain in statistical processing; $(m, n)$, current coordinates in the original image; NA, numerical aperture of the receiving lens; $\tilde{n}$, refractive index of the air; $N_v$, concentration of the scattering centers, % (see Table 1); PF and PV, frequency and intensity of pixels (see Fig. 7); $p_I(I)$, probability density for the speckle field intensity; $(p', q')$, cell number in the CCD matrix; $q$, image lens radius (see Figs. 3, 4); $\mathbf{r}$, $z$, spatial coordinates, m; $r_h$, characteristic size of correlation, m; $r_s$, average size of speckles, μm; $r_0$, $r_i$, one-dimensional transfer functions of the optical system; $t$, time, sec; $w$, current radius of the laser beam, m; $w_0$, laser beam radius in the waist (focus), mm; $\mathbf{x}$, $\mathbf{X}$, vectors in the object and image plane, respectively, m; $(x, y)$, coordinates in the object plane, m; $(x', y')$, coordinates in the image plane, m; $\alpha$, angle of incidence of radiation, rad (see Figs. 3, 4); $\delta(...)$, delta function; $\delta z$, depth of focus, μm; $\delta z_d$, diffraction term, μm; $\delta z_g$, geometrical correction, μm; $\delta z_{px}$, distance between sensitive elements in the CCD matrix, μm; $\zeta_0$, $\zeta_1$, speckle radii in the source plane and the diffuse object plane, respectively, μm (see Fig. 2); $\Theta$, probing radiation scattering angle, rad; $\theta_1$, $\theta_2$, parameters; $\lambda$, laser radiation wavelength in the medium, μm; $\lambda_0$, laser radiation wavelength in vacuum, μm; $(\nu, \omega)$, current coordinates in the Fourier plane; $\rho$, wavefront curvature, m; $\sigma_n$, experimental noise in the initial intensity of the speckle field, W/m$^2$; $\tilde{\sigma}_n$, experimental noise in the Fourier plane, W/m$^2$; $\sigma_I$, rms deviation of the laser radiation intensity in the subregion, W/m$^2$; $\tau$, time interval, sec; $\varphi_0$, initial phase difference, rad; $\Omega$, solid angle, sr; $\mathbb{C}(m, n)$, speckle field contrast; $\mathbb{F}\{...\}$, Fourier transform operator; $\mathfrak{J}_E$, $\mathfrak{J}_{\Delta I}$, autocorrelation functions for the fluctuating component of the laser radiation and the complex amplitude of the wave, respectively; $\mathfrak{M}$, optical magnification in specklogram recording; $\mathfrak{U}(\nu, \omega)$, radiation

power spectrum. Subscripts: d, diffraction; g, geometric; h, characteristic; L, lense; n, nois; p, particle; px, pixel; s, speckle; v, volume; 0, initial value of a physical quantity; 1, 2, 3, ..., ordinal values of physical quantities; $\langle ... \rangle$, mean value of a quantity; $*$, complex conjugation, transposition.

## REFERENCES


1. Nondestructive testing: http:// en.wikipedia.org/wiki/Nondestructive_testing.
2. F. J. Weinberg, *Optics of Flame*, Butterworth, London (1963).
3. W. Hauf and U. Grigull, Optical methods in heat transfer, *Adv. in Heat Transfer*, **6**, 133–366 (1970).
4. K. S. Shifrin, *Light Scattering in a Turbid Medium* [in Russian], GITTL, Moscow (1951).
5. L. A. Chernov, *Propagation of Waves in a Medium with Random Inhomogeneities* [in Russian], Izd. AN SSSR, Moscow (1958).
6. A. P. Ivanov, *Optics of Scattering Media* [in Russian], Nauka i Tekhnika, Minsk (1969).
7. H. C. Van de Hulst, *Light Scattering by Small Particles* [Russian translation], IL, Moscow (1961).
8. Yu. E. Nesterikhin and R. I. Soloukhin, *Rapid Measurements in the Gas Dynamics and Physics of Plasma* [in Russian], Nauka, Moscow (1967).
9. W. Merzkirch, *Flow Visualization*, 2nd edn., Academic Press, Orlando (1987).
10. T. S. Duranni and C. A. Grated, *Laser Systems in Flow Measurements* [Russian translation], Énergiya, Moscow (1980).
11. V. F. Klimkin, A. N. Panyrin, and R. I. Soloukhin, *Optical Methods of Recording Fast Processes* [in Russian], Nauka, Novosibirsk (1980).
12. R. K. Erf (Ed.), *Speckle Metrology*, Academic Press, New York (1978).
13. M. Francon, *La Granullarite Laser* (*Spekle*) *et ses Applications en Optique* [Russian translation], Mir, Moscow (1980).
14. R. S. Sirohi (Ed.), *Speckle Metrology*, Marcel Dekker Inc., New York (1993).
15. N. Fomin, *Speckle Photography for Fluid Mechanics Measurements*, Springer Verlag, Berlin (1998).
16. M. Raffel, C. E. Willert, and J. Kompenhans, *Particle Image Velocimetry: A Practical Guide*, Springer Verlag, Berlin (1998).
17. J. M. Burch and J. M. J. Tokarski, Production multiple beam fringes from photographic scatterers, *Optica Acta*, **15**, No. 2, 101–111 (1968).
18. A. Ya. Khairulina, Investigation of biocells by light-scattering methods, in: A. N. Ivanov (Ed.), *Light Propagation in a Disperse Medium* [in Russian], Nauka i Tekhnika, Minsk (1982), pp. 275–292.
19. G. Benedeck, Optical mixing spectroscopy and its applications to the problems of physics, chemistry, biology, and engineering, *Usp. Fiz. Nauk*, **106**, No. 3, 481–504 (1972).
20. H. Z. Cummins and E. R. Pike, *Photon Correlation and Light Beating Spectroscopy* [Russian translation], Mir, Moscow (1978).
21. J. D. Briers, Laser Doppler and time varying speckle: a reconciliation, *J. Opt. Soc. Am.*, **13**, 345–350 (1996).
22. N. B. Bazylev, E. I. Lavinskaya, and N. A. Fomin, Laser digital speckle anemometry of flows in the microchannels of fuel elements, *Inzh.-Fiz. Zh.*, **79**, NO. 6, 176–189 (2006).
23. N. B. Bazylev, E. I. Lavinskaya, S. A. Naumovich, S. P. Rubnikovich, and N. A. Fomin, Laser probing of biocells by the methods of dynamic quasi-real-time speckle photography, *Dokl. Nats. Akad. Nauk Belarusi*, **47**, No. 7, 46–50 (2003).
24. C. D. Meinhart, S. T. Wereley, and M. H. M. Gray, Volume illumination for two-dimensional particle image velocimetry, *Meas. Sci. Technol.*, **11**, 809–814 (2000).
25. C. D. Meinhart, S. T. Wereley, and J. G. Santiago, PIV measurements of a microchannel flow, *Exp. Fluids*, **27**, No. 5, 414–419 (1999).
26. J. P. Prenel, R. Porkar, and A. El. Rhassouli, Three-dimensional flow analysis by means of sequential and volumetric laser sheet illumination, *Exp. Fluids*, **7**, 133–137 (1989).
27. N. B. Bazylev, S. M. Vlasenko, E. I. Lavinskaya, and N. A. Fomin, quasi-real-time, Digital speckle photography of fast processes, *Dokl. Nats. Akad. Nauk Belarusi*, **45**, No. 5, 55–59 (2001).

28. T. Yoshimura, Statistical properties of dynamic speckles, *J. Opt. Soc. Am.*, **3**, 1032–1054 (1986).
29. J. C. Dainty (Ed.), *Laser Speckle and Related Phenomena*, Springer Verlag, Berlin (1984).
30. I. G. Stewart, *Introduction to Fourier Optics* [Russian translation], Mir, Moscow (1985).
31. E. I. Lavinskaya, S. Martem'yanov, J.-B. Solnier, and N. A. Fomin, Limited-projection laser tomography of combined gas-dynamic flows, *Inzh.-Fiz. Zh.*, **77**, No. 5, 94–104 (2004).